The Journal of Physical Chemistry Letters

pubs.acs.org/JPCL Letter

Biexciton Dynamics in Single Colloidal CdSe Quantum Dots

Bin Li, Guofeng Zhang,* Yong Zhang, Changgang Yang, Wenli Guo, Yonggang Peng, Ruiyun Chen, Chengbing Qin, Yan Gao, Jianyong Hu, Ruixiang Wu, Jie Ma, Haizheng Zhong, Yujun Zheng, Liantuan Xiao,* and Suotang Jia

Cite This: J. Phys. Chem. Lett. 2020, 11, 10425−10432 Read Online

ABSTRACT: The investigation of biexciton dynamics in single colloidal quantum dots (QDs) is critical to biexciton-based applications. Generally, a biexciton exhibits an extremely low photoluminescence (PL) quantum yield as well as very fast PL decay due to strong nonradiative Auger recombination, making it difficult to investigate the biexciton dynamics. Here, we develop a quantitative method based on intensity- and time-resolved photon statistics to investigate the biexciton dynamics in single colloidal QDs. This robust method can be used under high-excitation conditions to determine the absolute radiative and Auger recombination rates of both neutral and charged biexciton states in a single QD level, and the corresponding ratios between the two states agree with the theoretical predictions of the asymmetric band structures of CdSe-based QDs. Furthermore, the surface traps are found to provide additional nonradiative recombination pathways for the biexcitons, and their contributions are quantified by the method.

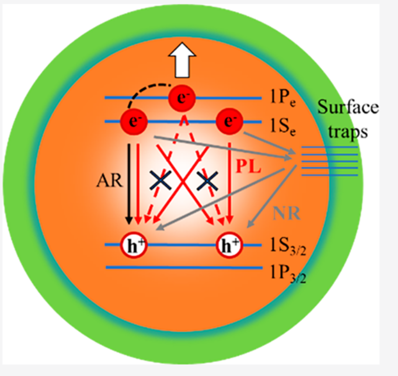

Many-particle effects, manifested as the formation of multiple excitons associated with Coulomb interactions among photoexcited electrons and holes, tend to be more significant in nanostructures than in bulk. The strong Coulomb interactions in a confined volume lead to a number of novel physical phenomena, including large splitting in electronic states,[1−3] enhanced intraband relaxation,[4] efficient carrier multiplication,[5] and ultrafast multiexciton decay.[6] Significant research interest in multiexciton phenomena has been stimulated by their relevance to emerging applications, such as quantum dot (QD)-based photovoltaics,[7] light-emitting diodes,[8,9] lasing,[10] and entangled photon-pair sources.[11,12] Because the multiexciton effects exhibit a nonlinear dependence on the exciton number,[13] often dominated by that of the biexciton contribution,[14] a clear understanding of biexciton dynamics, particularly separating the intrinsic and extrinsic effects, is pertinent for both fundamental physics and application aspects.

The intrinsic and extrinsic effects, such as extra charges and surface states, that commonly exist in QDs strongly affect the exciton dynamics. When an extra charge is generated in the QD, the charged single exciton becomes less emissive because its energy would likely be transferred to the extra electron or hole through a nonradiative Auger process.[15−18] The surface traps can also provide nonradiative channels to reduce the photoluminescence (PL) quantum yield (QY) of the single neutral exciton.[19−24] The formation of the charged states and the presence of surface traps can also result in Auger blinking and band-edge carrier (BC) blinking, respectively.[25] Although the techniques for characterization of the single exciton are relatively mature and the underlying physics is also fairly well understood, the situation for multiple excitons, even biexciton, is very different. Compared to the single exciton, the biexciton has an extremely low generation probability and PLQY as well as very fast PL decay due to the strong nonradiative Auger recombination.[26−30] However, biexciton dynamics can be investigated through different experimental methods. For example, the biexciton decay curve was extracted from the PL decay by subtracting the single exciton component measured at low pump fluences in ensemble transient absorption spectroscopy.[31−33] The biexciton lifetime could also be obtained by photon correlation methods in the ensemble or a single-particle level.[34−36] The biexciton QY was most often estimated with a second-order correlation function [$g^{(2)}$] method by combining it with the single-exciton QY in single-dot spectroscopy in a weak excitation limit.[26,37] Upon simultaneous measurement of both the $g^{(2)}$ and PL-decay curves, the biexciton QY can be determined even under higher-excitation conditions.[27] Because of the presence of extra charges and surface states and the weaker signal, properly characterizing the biexciton state to quantify the contributions of the intrinsic effects (e.g., radiative and Auger process) and extrinsic effect (e.g., nonradiative recombination through surface traps) on a single-QD level remains challenging.

Received: September 16, 2020
Accepted: November 5, 2020

https://dx.doi.org/10.1021/acs.jpclett.0c02832
J. Phys. Chem. Lett. 2020, 11, 10425−10432

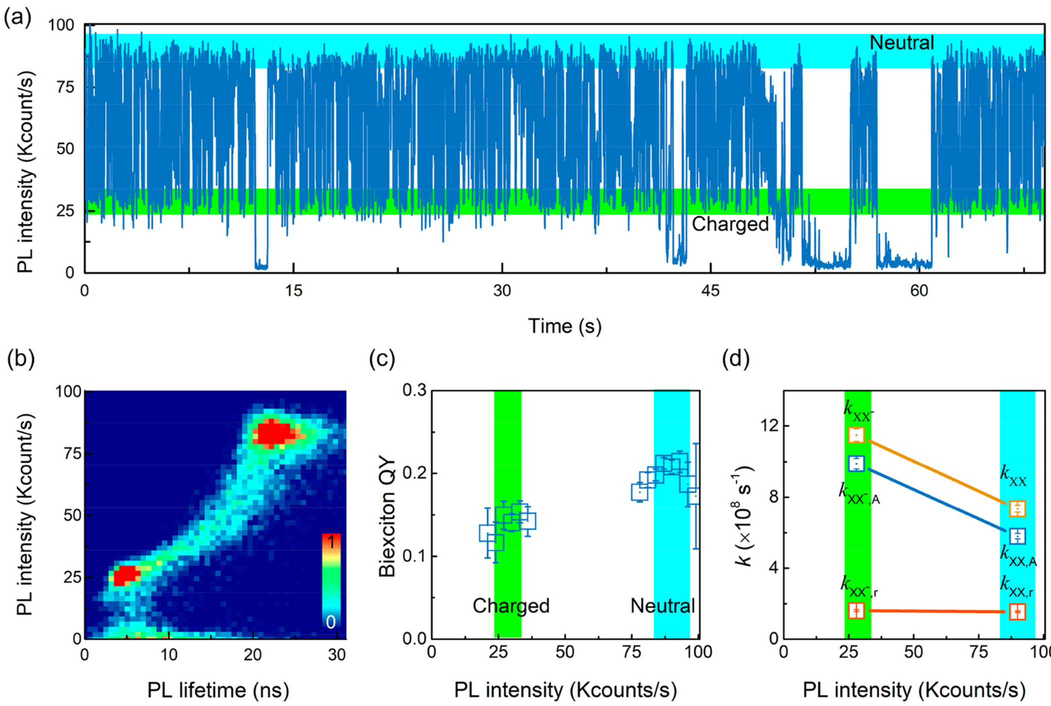

Figure 1. Biexciton QYs and radiative and nonradiative rates in a single QD in neutral and charged states. (a) Typical PL trajectory for a single QD with a binning time of 10 ms, where PL blinking originates from the charging and discharging of the QD. (b) Corresponding FLID in color scale. (c) Corresponding charged and neutral biexciton QYs. (d) Corresponding total decay rates, radiative rates, and Auger rates of the charged and neutral biexcitons.

In this work, we investigate the biexciton dynamics in single colloidal QDs by a quantitative method based on intensity- and time-resolved photon statistics. The method allows a single QD to be excited under a higher-excitation condition to obtain the absolute biexciton QY, independent of the single exciton QY, PL-decay curves, etc. With this method, biexciton QYs can be extracted from different intensity levels of the PL time trajectory to investigate the biexciton dynamics. Our approach provides the experimental investigation of the absolute radiative and Auger nonradiative recombination rates of neutral and charged biexciton states in a single QD level. In particular, for the first time, we extend the analysis of the nonradiative recombination process caused by surface traps from a single exciton to a biexciton.

To study the biexciton dynamics in single colloidal QDs, a confocal microscope combined with a Hanbury Brown-Twiss (HBT) detection scheme is used for photon statistics (detailed information can be found in section S1 and Figure S1). A time-tagged, time-resolved, and time-correlated single-photon counting data acquisition card is employed to record the absolute arrival time of each photon with picosecond time resolution. The detection of either one or two photons after each excitation pulse is used to distinguish the single- or two-photon event, respectively. The rates of single- and two-photon events, denoted as N_1 and N_2, respectively, can be expressed as (the detailed information can be found in section S2 and Figures S2 and S3)

$$N_1 = FP_X Q_X \times 2\xi \tag{1}$$

$$N_2 = FP_{XX} Q_{XX} Q_X \times 2\xi^2 \tag{2}$$

where F is the repetition frequency of the pulsed laser, P_X and P_{XX} are the probabilities of populating the single exciton and biexciton states in the QDs, respectively, Q_X and Q_{XX} are the single exciton and biexciton QYs, respectively, and ξ is the detection efficiency of each optical detection path in the HBT detection scheme. The value of ξ is ~0.075 for the two detection paths in our system (detailed information can be found in section S1).[38] P_X and P_{XX} are described by Poisson distributions:[26]

$$P_X = \sum_{m=1}^{\infty} P(\langle N\rangle, m) = 1 - e^{-\langle N\rangle} \tag{3}$$

$$P_{XX} = \sum_{m=2}^{\infty} P(\langle N\rangle, m) = 1 - e^{-\langle N\rangle} - \langle N\rangle e^{-\langle N\rangle} \tag{4}$$

where $\langle N\rangle$ is the average number of photons absorbed per QD per pulse[26,27,39] and can be obtained by fitting the PL saturation curve with the inverse exponential $(1 - e^{\langle N\rangle})$.[39−41] To obtain a more accurate $\langle N\rangle$ value, the multiexciton emission photons should be removed from the PL saturation curve by the time-gating method,[42−44] and then a single-exciton saturation curve can be constructed to be fitted to obtain the $\langle N\rangle$ value (detailed information can be found in section S3 and Figure S4).

From eqs 1−4, the biexciton QY can be described as

$$Q_{XX} = \left\{\left[1 - \frac{\langle N\rangle \exp(-\langle N\rangle)}{1 - \exp(-\langle N\rangle)}\right]\xi\right\}^{-1} \times \frac{N_2}{N_1} \tag{5}$$

Therefore, the biexciton QY is determined by the rates of single- and two-photon events (N_1 and N_2, respectively), as shown in Figure S5. Compared to the $g^{(2)}$ method,[26,37] the method overcomes the limitation of the weak excitation condition ($\langle N\rangle \to 0$) to allow a single QD to be excited with a higher-excitation condition ($\langle N\rangle$ can be up to ~0.64), which is

https://dx.doi.org/10.1021/acs.jpclett.0c02832
J. Phys. Chem. Lett. 2020, 11, 10425−10432

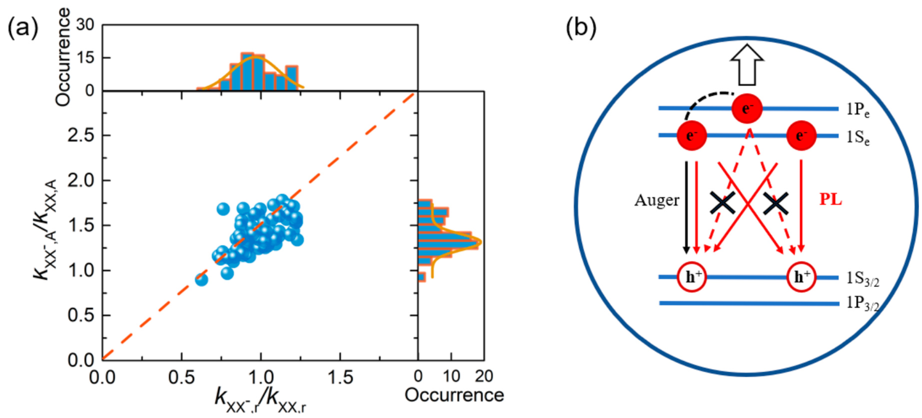

Figure 2. Ratios and schematic for both radiative recombination and Auger nonradiative recombination rates of the charged and neutral biexciton states. (a) Statistical distribution of the ratio of radiative rates ($k_{XX^-,r}/k_{XX,r}$) and of Auger nonradiative rates ($k_{XX^-,A}/k_{XX,A}$) between charged and neutral biexciton states for ∼78 single QDs. The histograms of $k_{XX^-,r}/k_{XX,r}$ and $k_{XX^-,A}/k_{XX,A}$ with Gaussian fitting are shown along the horizontal (top) and vertical (right) axes, respectively. (b) Schematic of radiative recombination pathways and Auger nonradiative recombination of the charged biexciton state for a CdSe-based QD.

important, because most practical applications would not be in the weak excitation limit. This method allows for higher-excitation conditions because the ratio of N_2 and N_1 in eq 5 can reduce the deviation of the calculation result of biexciton QY (detailed information can be found in section S2 and Figures S2 and S3). In addition, by taking the single-exciton saturation curve in a time-gated fashion without contributions from multiexcitons, we can accurately obtain the corresponding ⟨N⟩ value, so the calculation accuracy of the biexciton QY can be further improved. Under the higher-excitation condition, the method allows us to extract the absolute biexciton QY from different intensity levels of the PL time trajectory. Therefore, a detailed intensity-dependent evolution of biexciton dynamics as well as the effects of extra charges and surface traps on biexciton dynamics can be obtained by the method.

Before the investigation of the effects of extra charges and surface traps on biexciton dynamics, it is necessary to distinguish whether there are extra charges or surface traps in a single QD and to dominate the exciton dynamics. The extra charges and the surface traps can be distinguished by the blinking mechanisms, because the charging and discharging of QD result in Auger blinking, and the activation and deactivation of surface traps result in BC blinking.[25]

A typical PL intensity trajectory of a single QD (alloyed $CdSe/Cd_xZn_{1-x}S$ core/shell QDs) at ⟨N⟩ = 0.12 is shown in Figure 1a. The transmission electron microscope (TEM) image, absorption and emission spectra of the QDs, and the method for sample preparation are presented in section S4 and Figures S6 snd S7). Upon calculation of the average lifetime of each bin, the corresponding fluorescence lifetime−intensity distribution (FLID) can be obtained as shown in Figure 1b. The PL intensities of 90K counts/s (blue region) and 27K counts/s (green region) correspond to lifetime values of 23 and 4 ns, respectively. Therefore, the ratio of radiative rates between the green and blue regions is ∼2, indicating that the observed PL blinking is Auger blinking (involving extra charge), which originates from the charging and discharging of the QD.[25] Consequently, the blue and green regions correspond to the neutral and negatively charged states, respectively. Using eq 5, the biexciton QY as a function of PL intensity can be obtained as shown in Figure 1c. Each square in the figure represents a biexciton QY value obtained for one PL intensity level (with an interval of 3K counts/s). The biexciton QYs are calculated by the values of N_1 and N_2 that are extracted for different intensity levels. The error bars are caused by the shot noise of photon counting.[45] The average QYs of the charged and neutral biexciton are ∼0.15 and ∼0.21, respectively. Upon analysis of the corresponding biexciton lifetimes obtained by a first photon analysis,[46] the absolute biexciton radiative and Auger rates of each state (Figure 1d) can be calculated (see details in section S5), and the error bars are derived from the fitting of the decay curves, as shown in Figure S8. From Figure 1d, we can determine that the Auger rate of the charged biexciton ($k_{XX^-,A}$) is ∼1.7 times that of the neutral biexciton ($k_{XX,A}$), and the ratio of the radiative rates between the neutral biexciton and charged biexciton ($k_{XX^-,r}/k_{XX,r}$) is ∼1.0. The correlations between the ratio of the radiative rates ($k_{XX^-,r}/k_{XX,r}$) and that of the Auger rates ($k_{XX^-,A}/k_{XX,A}$) for ∼78 single QDs are presented in Figure 2a. The histograms of $k_{XX^-,r}/k_{XX,r}$ and $k_{XX^-,A}/k_{XX,A}$ values are fitted by Gaussian functions with values of 0.96 ± 0.03 and 1.32 ± 0.02, respectively.

These values can be compared with the expected values for CdSe-based QDs obtained using an asymmetric band structure model.[47,48] The charged biexciton has 2-fold degenerate $1S_e$ levels, and the extra electron resides in the $1P_e$ state,[48] as shown in Figure 2b. The interband transitions are forbidden, as indicated by red dotted arrows. There are four radiative pathways for the charged biexciton highlighted by the red arrows in Figure 2b, which is same as that of the neutral biexciton. Therefore, the theoretical value of $k_{XX^-,r}/k_{XX,r}$ is ∼1, which agrees with the experimental result of 0.96. The Auger event is the recombination of one $1S_e$ electron and one $1S_{3/2}$ hole accompanied by re-excitation of another charge carrier (including the $1P_e$ electron as indicated by the black dotted line in Figure 2b). The schematic illustration presents twelve Auger pathways for the charged biexciton and eight Auger pathways for the neutral biexciton. Hence, the expected ratio of Auger rates between charged and neutral biexcitons should be 1.5 with a presumption that all of the Auger pathways are equal in probability, closely resembling the value of 1.32 obtained in our experiment.

https://dx.doi.org/10.1021/acs.jpclett.0c02832
J. Phys. Chem. Lett. 2020, 11, 10425−10432

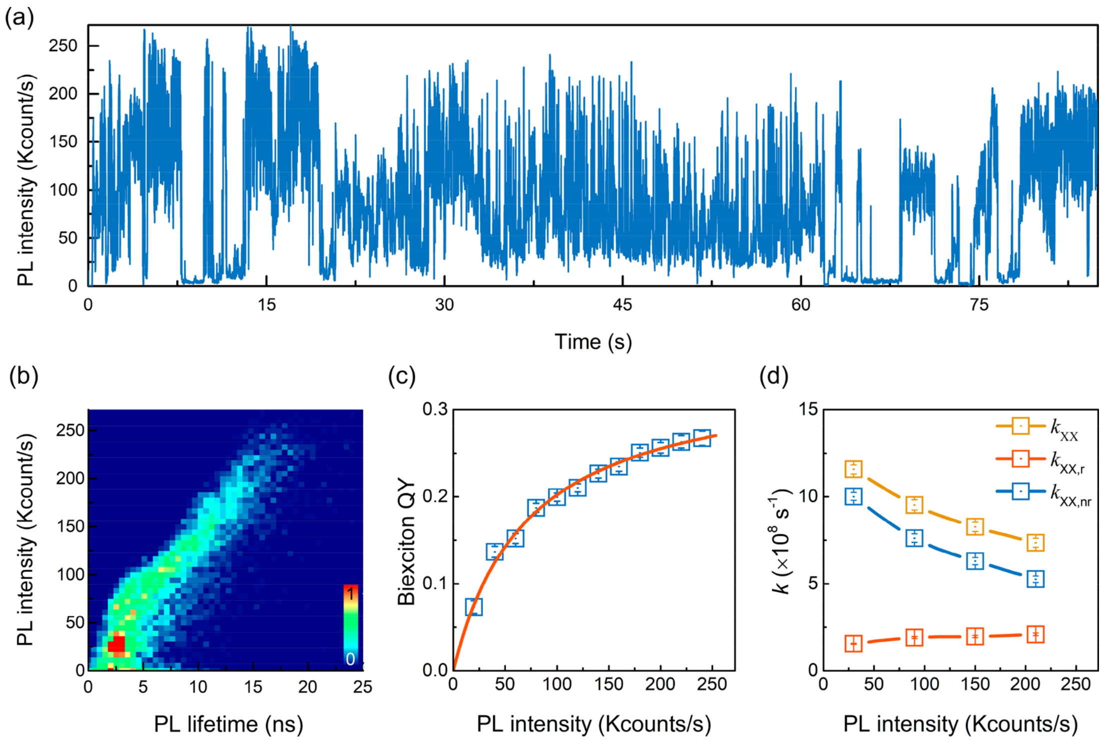

Figure 3. Effects of surface traps on biexciton QYs and radiative and nonradiative rates in a single QD. (a) Typical PL trajectory for a single QD with a binning time of 10 ms and PL blinking that originated from the activation and deactivation of surface traps. (b) Corresponding FLID in color scale. (c) Biexciton QY as a function of PL intensity for the PL trajectory in panel a and a fitted curve (red line). (d) Corresponding total decay rate (k_{xx}), radiative rate ($k_{xx,r}$), and nonradiative rate ($k_{xx,nr}$) of the biexciton as a function of PL intensity.

Another type of blinking trajectory of the single QDs with an $\langle N \rangle$ of 0.3 is shown in Figure 3a, different from that in Figure 1. The corresponding FLID (Figure 3b) presents a linear correlation between the PL intensity and the lifetime, which means that the ratio between each state is 1. This type of blinking is BC blinking, which originates from the activation and deactivation of surface traps. BC blinking can be explained by the multiple-recombination center (MRC) model,[19,25,49] which assumes that the MRCs are distributed on the QD surface; the single exciton state can either relax via a radiative pathway and emit a photon or decay nonradiatively through activated MRCs. These MRCs are short-lived shallow traps, and the time scale of trapping and nonradiative recombination is close to that of radiative recombination of the band-edge exciton.[25,49] At the bright state of PL intensity trajectories, the QD mainly cycles between photon absorption to create an exciton and radiative recombination, and radiative rate $k_{X,r}$ is much higher than nonradiative recombination rate $k_{X,nr}$. The $k_{X,nr}$ is determined by the number of activated MRCs. When more MRCs are activated simultaneously, the $k_{X,nr}$ becomes higher, and the PL intensity of QDs will be further reduced. According to eq 5, the biexciton QY (Q_{XX}) as a function of PL intensity can be obtained as shown in Figure 3c, which can be fitted by taking into account both the Auger process and the surface trapping of biexcitons, as will be discussed later. Applying the first photon analysis,[46,50] we can obtain the biexciton lifetime (τ_{XX}) for each PL intensity level, as shown in Figure S9. The decay rate of each PL intensity level can be obtained from the value of τ_{XX} and the corresponding value of Q_{XX}, as shown in Figure 3d (see details in section S5). It shows that the nonradiative rate of the biexciton ($k_{XX,nr}$) increases when the PL intensity decreases, while the radiative rate of the biexciton ($k_{XX,r}$) remains constant.

Because the surface traps strongly affect the PL emission of a single exciton, the single-exciton PLQY can be expressed as

$$Q_X = k_{X,r}/(k_{X,r} + k_{X,nr}) \tag{6}$$

We anticipate that the surface traps also affect the biexciton recombination. For a quantitative insight into the effect of surface traps on the biexciton dynamics, we fit the data points in the Figure 3c with the consideration of the contributions from both the Auger recombination and the surface traps. The biexciton QY can be expressed as

$$Q_{XX} = k_{XX,r}/(k_{XX,r} + k_{XX,A} + k_{XX,nr,trap}) \tag{7}$$

where $k_{XX,nr,tap}$ is the nonradiative recombination rate of the biexciton through the surface traps. Biexciton radiative rate $k_{XX,r}$ is theoretically considered to be 4 times that of the single exciton in previous reports.[34,35,48,50−52] However, this ratio of radiative rates also depends on the shell thickness of the QD,[53] so that we give a more general expression to be

$$k_{XX,r} = \alpha k_{X,r} \tag{8}$$

Consistent with previous reports,[25,50] $k_{X,r}$ remains constant for the BC-blinking trajectory in Figure 3a. $k_{X,r}$ can be determined to be 5.6×10^7 s^{-1} by the single-exciton QY and lifetime. Therefore, upon combination of $k_{X,r}$ with $k_{XX,r}$ in Figure 3d, $\alpha = k_{XX,r}/k_{X,r} = 3.7$ for the single QD in Figure 3. More values of α for other single QDs can be obtained in the same way.

Similarly, the biexciton nonradiative rate through the surface traps can be expressed as

$$k_{XX,nr,trap} = \beta k_{X,nr} \tag{9}$$

https://dx.doi.org/10.1021/acs.jpclett.0c02832
J. Phys. Chem. Lett. 2020, 11, 10425−10432

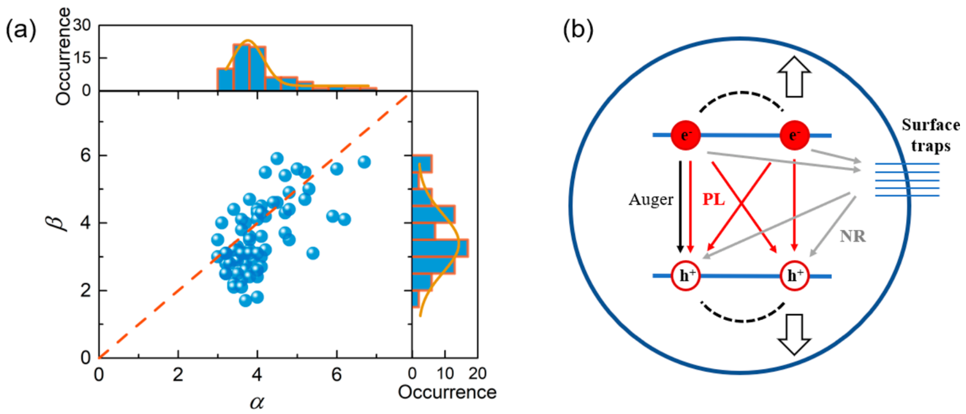

Figure 4. Ratios and schematic for both radiative recombination and nonradiative recombination rates. (a) Statistical distributions of α ($\alpha = k_{xx,r}/k_{xx,r}$) and β ($\beta = k_{xx,nr,tap}/k_{x,nr}$) plotted for ∼72 single QDs. The histograms of α and β with Gaussian fitting are shown along the horizontal (top) and vertical (right) axes, respectively. (b) Schematic of radiative recombination pathways (red arrows) and Auger and surface nonradiative recombination processes for the biexciton state.

Because the value of N_1 is approximately equal to PL intensity (I), it can be obtained from eqs 6−9 that

$$Q_{XX} = \left(1 - \frac{\beta}{\alpha} + \frac{1}{\alpha}\frac{k_{XX,A}}{k_{X,r}} + \frac{\beta}{\alpha}\frac{FP_X \times 2\xi}{I}\right)^{-1} \tag{10}$$

where $k_{XX,A}$ is mainly influenced by the shell thickness of the QD and is considered to be a constant for each PL intensity level.[30] Then, Q_{XX} as a function of PL intensity (I) (Figure 3c) can be fitted by eq 10 with a β of 3.2. More values of β for other single QDs were obtained in the same way. The statistical distributions of α and β obtained for ∼72 single QDs are summarized in Figure 4a. The histograms of α and β are fitted by Gaussian functions with values of 3.76 ± 0.04 and 3.40 ± 0.22, respectively.

Next, we discuss the values of α and β with a theoretical model shown schematically in Figure 4b. The single-exciton state has one radiative pathway, while the biexciton state has four radiative pathways (red arrows in Figure 4b). Therefore, the theoretical ratio of radiative rates between the biexciton and single exciton (α) equals 4.[48] The experimental result of 3.76 ± 0.04 is close to the theoretical prediction. The theoretical value of 4 was also demonstrated in CdSe/CdS QDs by using photon correlation methods.[34] For the single-exciton state, there would be only one nonradiative pathway provided by surface traps. For the biexciton state, the surface traps capture an electron through two nonradiative pathways, and subsequently, the electron captured by the surface recombines nonradiatively with the hole in the core through two other pathways, as illustrated by gray arrows in Figure 4b. Therefore, there would be four nonradiative pathways provided by the surface traps. Consequently, the theoretical value of β should be 4. The deviation of the experimental value of β (3.40 ± 0.22), as well as α (3.76 ± 0.04), from the theoretical value may be attributed to the inadequate system time resolution, the involvement of higher-order multiexcitons, or the difference in the single-exciton and biexciton dipole moments.[54]

In summary, we have developed a robust quantitative method based on intensity- and time-resolved photon statistics for investigating the biexciton dynamics in single QDs. This method can be used under high-excitation conditions in comparison to the established $g^{(2)}$ method. With this method, the absolute biexciton QYs and radiative, Auger, and surface nonradiative rates of single QDs have been obtained and correlated with PL intensities. The validity of the results is further supported by the consistency between the experimental results and theoretical expectations for multiple ratios of recombination rates: between the charged and neutral biexciton state, the ratio of radiative rates of ∼1.32 (experiment) versus 1.5 (theory), and the ratio of Auger recombination rates of ∼0.96 versus 1.0; between biexciton and single exciton, the ratio of radiative rates of ∼3.76 versus 4 and surface recombination rates of ∼3.40 versus 4. This method can also be applied to other challenging problems, for instance, the effect of plasmonic nanostructures on the biexciton dynamics, confirmation of carrier multiplication, and estimation of the generation efficiency of the biexciton. Although when the excitation power is further increased, the results obtained by this method will gradually deviate from the correct values, by using multidetectors and considering the contribution of multiexcitons, this method can be extended to allow even higher-excitation conditions than the current implementation and used to investigate the higher-order exciton dynamics.

■ ASSOCIATED CONTENT

Supporting Information

The Supporting Information is available free of charge at https://pubs.acs.org/doi/10.1021/acs.jpclett.0c02832.

> Sample preparation and experimental setup, TEM image of QDs, absorption and PL spectra of QDs, evaluating the excitation power allowed by the method, estimation of the value of ⟨N⟩, method for obtaining biexciton rates, blinking trajectories, FLID, and $g^{(2)}$ curves of single QDs with different excitation powers (PDF)

■ AUTHOR INFORMATION

Corresponding Authors

Guofeng Zhang − *State Key Laboratory of Quantum Optics and Quantum Optics Devices, Institute of Laser Spectroscopy, Collaborative Innovation Center of Extreme Optics, Shanxi University, Taiyuan 030006, China;* orcid.org/0000-0002-9030-0431; Email: guofeng.zhang@sxu.edu.cn

Liantuan Xiao − *State Key Laboratory of Quantum Optics and Quantum Optics Devices, Institute of Laser Spectroscopy, Collaborative Innovation Center of Extreme Optics, Shanxi*

https://dx.doi.org/10.1021/acs.jpclett.0c02832
J. Phys. Chem. Lett. 2020, 11, 10425−10432

University, Taiyuan 030006, China; orcid.org/0000-0003-2690-6460; Email: xlt@sxu.edu.cn

Authors

Bin Li − *State Key Laboratory of Quantum Optics and Quantum Optics Devices, Institute of Laser Spectroscopy, Collaborative Innovation Center of Extreme Optics, Shanxi University, Taiyuan 030006, China; Key Laboratory of Spectral Measurement and Analysis of Shanxi Province, College of Physics and Information Engineering, Shanxi Normal University, Linfen 041004, China;* orcid.org/0000-0002-5817-6792

Yong Zhang − *Department of Electrical and Computer Engineering, University of North Carolina at Charlotte, Charlotte, North Carolina 28223, United States;* orcid.org/0000-0003-4781-1583

Changgang Yang − *State Key Laboratory of Quantum Optics and Quantum Optics Devices, Institute of Laser Spectroscopy, Collaborative Innovation Center of Extreme Optics, Shanxi University, Taiyuan 030006, China;* orcid.org/0000-0003-1063-8975

Wenli Guo − *State Key Laboratory of Quantum Optics and Quantum Optics Devices, Institute of Laser Spectroscopy, Collaborative Innovation Center of Extreme Optics, Shanxi University, Taiyuan 030006, China*

Yonggang Peng − *School of Physics, Shandong University, Jinan 250100, China*

Ruiyun Chen − *State Key Laboratory of Quantum Optics and Quantum Optics Devices, Institute of Laser Spectroscopy, Collaborative Innovation Center of Extreme Optics, Shanxi University, Taiyuan 030006, China;* orcid.org/0000-0002-0037-856X

Chengbing Qin − *State Key Laboratory of Quantum Optics and Quantum Optics Devices, Institute of Laser Spectroscopy, Collaborative Innovation Center of Extreme Optics, Shanxi University, Taiyuan 030006, China;* orcid.org/0000-0002-6822-5113

Yan Gao − *State Key Laboratory of Quantum Optics and Quantum Optics Devices, Institute of Laser Spectroscopy, Collaborative Innovation Center of Extreme Optics, Shanxi University, Taiyuan 030006, China*

Jianyong Hu − *State Key Laboratory of Quantum Optics and Quantum Optics Devices, Institute of Laser Spectroscopy, Collaborative Innovation Center of Extreme Optics, Shanxi University, Taiyuan 030006, China*

Ruixiang Wu − *Key Laboratory of Spectral Measurement and Analysis of Shanxi Province, College of Physics and Information Engineering, Shanxi Normal University, Linfen 041004, China;* orcid.org/0000-0002-9273-0451

Jie Ma − *State Key Laboratory of Quantum Optics and Quantum Optics Devices, Institute of Laser Spectroscopy, Collaborative Innovation Center of Extreme Optics, Shanxi University, Taiyuan 030006, China*

Haizheng Zhong − *Beijing Key Laboratory of Nanophotonics and Ultrafine Optoelectronic Systems, School of Materials Science and Engineering, Beijing Institute of Technology, Beijing 100081, China;* orcid.org/0000-0002-2662-7472

Yujun Zheng − *School of Physics, Shandong University, Jinan 250100, China;* orcid.org/0000-0001-9974-2917

Suotang Jia − *State Key Laboratory of Quantum Optics and Quantum Optics Devices, Institute of Laser Spectroscopy, Collaborative Innovation Center of Extreme Optics, Shanxi University, Taiyuan 030006, China*

Complete contact information is available at: https://pubs.acs.org/10.1021/acs.jpclett.0c02832

Author Contributions

G.Z. and L.X. conceived and designed the experiments. B.L., C.Y., and W.G. performed the experiments, B.L. analyzed the data. B.L., Y. Zhang, G.Z., R.C., C.Q., H.Z., and L.X. co-wrote the manuscript. All authors discussed the results and commented on the manuscript at all stages.

Notes

The authors declare no competing financial interest.

■ ACKNOWLEDGMENTS

This work was supported by the National Key R&D Program of China (2017YFA0304203), the National Natural Science Foundation of China (62075120, 61527824, 61675119, 61875109, 91950109, and 61805134), PCSIRT (IRT_13076), PTIT, 1331KSC, and 111 project (Grant D18001). Y. Zhang was supported by the Bissell Distinguished Professorship at the University of North Carolina at Charlotte.

■ REFERENCES

(1) Yin, C. Y.; Chen, L. Y.; Song, N.; Lv, Y.; Hu, F. R.; Sun, C.; Yu, W. W.; Zhang, C. F.; Wang, X. Y.; Zhang, Y.; et al. Bright-Exciton Fine-Structure Splittings in Single Perovskite Nanocrystals. *Phys. Rev. Lett.* **2017**, *119*, 026401.

(2) Zhang, G. F.; Yang, C. G.; Ge, Y.; Peng, Y. G.; Chen, R. Y.; Qin, C. B.; Gao, Y.; Zhang, L.; Zhong, H. Z.; Zheng, Y. J.; et al. Influence of Surface Charges on the Emission Polarization Properties of Single CdSe/CdS Dot-in-Rods. *Front. Phys.* **2019**, *14*, 63601.

(3) Zhang, G. F.; Peng, Y. G.; Xie, H. Q.; Li, B.; Li, Z. J.; Yang, C. G.; Guo, W. L.; Qin, C. B.; Chen, R. Y.; Gao, Y.; et al. Linear Dipole Behavior of Single Quantum Dots Encased in Metal Oxide Semiconductor Nanoparticles Films. *Front. Phys.* **2019**, *14*, 23605.

(4) Klimov, V. I.; McBranch, D. W. Femtosecond 1P-to-1S Electron Relaxation in Strongly Confined Semiconductor Nanocrystals. *Phys. Rev. Lett.* **1998**, *80*, 4028−4031.

(5) Witzel, W. M.; Shabaev, A.; Hellberg, C. S.; Jacobs, V. L.; Efros, A. L. Quantum Simulation of Multiple-Exciton Generation in a Nanocrystal by a Single Photon. *Phys. Rev. Lett.* **2010**, *105*, 137401.

(6) Klimov, V. I.; McGuire, J. A.; Schaller, R. D.; Rupasov, V. I. Scaling of Multiexciton Lifetimes in Semiconductor Nanocrystals. *Phys. Rev. B: Condens. Matter Mater. Phys.* **2008**, *77*, 195324.

(7) Yang, W. S.; Park, B. W.; Jung, E. H.; Jeon, N. J.; Kim, Y. C.; Lee, D. U.; Shin, S. S.; Seo, J.; Kim, E. K.; Noh, J. H.; et al. Iodide Management in Formamidinium-Lead-Halide-Based Perovskite Layers for Efficient Solar Cells. *Science* **2017**, *356*, 1376−1379.

(8) Xiao, Z. G.; Kerner, R. A.; Zhao, L. F.; Tran, N. L.; Lee, K. M.; Koh, T. W.; Scholes, G. D.; Rand, B. P. Efficient Perovskite Light-Emitting Diodes Featuring Nanometre-Sized Crystallites. *Nat. Photonics* **2017**, *11*, 108−115.

(9) Shen, X. Y.; Zhang, Y.; Kershaw, S. V.; Li, T. S.; Wang, C. C.; Zhang, X. Y.; Wang, W. Y.; Li, D. G.; Wang, Y. H.; Lu, M.; et al. Zn-Alloyed $CsPbI_3$ Nanocrystals for Highly Efficient Perovskite Light-Emitting Devices. *Nano Lett.* **2019**, *19*, 1552−1559.

(10) Klimov, V. I.; Mikhailovsky, A. A.; Xu, S.; Malko, A.; Hollingsworth, J. A.; Leatherdale, C. A.; Eisler, H. J.; Bawendi, M. G. Optical Gain and Stimulated Emission in Nanocrystal Quantum Dots. *Science* **2000**, *290*, 314−317.

(11) Fattal, D.; Inoue, K.; Vuckovic, J.; Santori, C.; Solomon, G. S.; Yamamoto, Y. Entanglement Formation and Violation of Bell's Inequality with a Semiconductor Single Photon Source. *Phys. Rev. Lett.* **2004**, *92*, 037903.

(12) Aichele, T.; Tribu, A.; Sallen, G.; Bocquel, J.; Bellet-Amalric, E.; Bougerol, C.; Poizat, J. P.; Kheng, K.; Andre, R.; Tatarenko, S.; et al.

CdSe Quantum Dots in ZnSe Nanowires as Efficient Source for Single Photons up to 220 K. *J. Cryst. Growth* **2009**, *311*, 2123−2127.

(13) Franceschetti, A.; Zhang, Y. Multiexciton Absorption and Multiple Exciton Generation in CdSe Quantum Dots. *Phys. Rev. Lett.* **2008**, *100*, 136805.

(14) Hu, F. R.; Lv, B. H.; Yin, C. Y.; Zhang, C. F.; Wang, X. Y.; Lounis, B.; Xiao, M. Carrier Multiplication in a Single Semiconductor Nanocrystal. *Phys. Rev. Lett.* **2016**, *116*, 106404.

(15) Efros, A. L.; Rosen, M. Random Telegraph Signal in the Photoluminescence Intensity of a Single Quantum Dot. *Phys. Rev. Lett.* **1997**, *78*, 1110−1113.

(16) Yang, C. G.; Zhang, G. F.; Feng, L. H.; Li, B.; Li, Z. J.; Chen, R. Y.; Qin, C. B.; Gao, Y.; Xiao, L. T.; Jia, S. T. Suppressing the Photobleaching and Photoluminescence Intermittency of Single Near-Infrared CdSeTe/ZnS Quantum Dots with *P*-Phenylenediamine. *Opt. Express* **2018**, *26*, 11889−11902.

(17) Thomas, E. M.; Ghimire, S.; Kohara, R.; Anil, A. N.; Yuyama, K.-I.; Takano, Y.; Thomas, K. G.; Biju, V. Blinking Suppression in Highly Excited CdSe/ZnS Quantum Dots by Electron Transfer under Large Positive Gibbs (Free) Energy Change. *ACS Nano* **2018**, *12*, 9060−9069.

(18) Hamada, M.; Nakanishi, S.; Itoh, T.; Ishikawa, M.; Biju, V. Blinking Suppression in CdSe/ZnS Single Quantum Dots by TiO_2 Nanoparticles. *ACS Nano* **2010**, *4*, 4445−4454.

(19) Frantsuzov, P. A.; Volkan-Kacso, S.; Janko, B. Model of Fluorescence Intermittency of Single Colloidal Semiconductor Quantum Dots Using Multiple Recombination Centers. *Phys. Rev. Lett.* **2009**, *103*, 207402.

(20) Li, B.; Zhang, G. F.; Wang, Z.; Li, Z. J.; Chen, R. Y.; Qin, C. B.; Gao, Y.; Xiao, L. T.; Jia, S. T. Suppressing the Fluorescence Blinking of Single Quantum Dots Encased in N-Type Semiconductor Nanoparticles. *Sci. Rep.* **2016**, *6*, 32662.

(21) Yuan, H.; Debroye, E.; Caliandro, G.; Janssen, K. P.; van Loon, J.; Kirschhock, C. E.; Martens, J. A.; Hofkens, J.; Roeffaers, M. B. Photoluminescence Blinking of Single-Crystal Methylammonium Lead Iodide Perovskite Nanorods Induced by Surface Traps. *ACS Omega* **2016**, *1*, 148−159.

(22) Tian, Y. X.; Merdasa, A.; Peter, M.; Abdellah, M.; Zheng, K. B.; Ponseca, C. S.; Pullerits, T.; Yartsev, A.; Sundstrom, V.; Scheblykin, I. G. Giant Photoluminescence Blinking of Perovskite Nanocrystals Reveals Single-Trap Control of Luminescence. *Nano Lett.* **2015**, *15*, 1603−1608.

(23) Wang, S. X.; Wang, Y.; Zhang, Y.; Zhang, X. T.; Shen, X. Y.; Zhuang, X. W.; Lu, P.; Yu, W. W.; Kershaw, S. V.; Rogach, A. L. Cesium Lead Chloride/Bromide Perovskite Quantum Dots with Strong Blue Emission Realized Via a Nitrate-Induced Selective Surface Defect Elimination Process. *J. Phys. Chem. Lett.* **2019**, *10*, 90−96.

(24) Huang, H.; Bodnarchuk, M. I.; Kershaw, S. V.; Kovalenko, M. V.; Rogach, A. L. Lead Halide Perovskite Nanocrystals in the Research Spotlight: Stability and Defect Tolerance. *ACS Energy Lett.* **2017**, *2*, 2071−2083.

(25) Yuan, G.; Gómez, D. E.; Kirkwood, N.; Boldt, K.; Mulvaney, P. Two Mechanisms Determine Quantum Dot Blinking. *ACS Nano* **2018**, *12*, 3397−3405.

(26) Ihara, T. Biexciton Cascade Emission Reveals Absolute Absorption Cross Section of Single Semiconductor Nanocrystals. *Phys. Rev. B: Condens. Matter Mater. Phys.* **2016**, *93*, 235442.

(27) Hiroshige, N.; Ihara, T.; Kanemitsu, Y. Simultaneously Measured Photoluminescence Lifetime and Quantum Yield of Two-Photon Cascade Emission on Single CdSe/ZnS Nanocrystals. *Phys. Rev. B: Condens. Matter Mater. Phys.* **2017**, *95*, 245307.

(28) Klimov, V. I.; Mikhailovsky, A. A.; McBranch, D. W.; Leatherdale, C. A.; Bawendi, M. G. Quantization of Multiparticle Auger Rates in Semiconductor Quantum Dots. *Science* **2000**, *287*, 1011−1013.

(29) Robel, I.; Gresback, R.; Kortshagen, U.; Schaller, R. D.; Klimov, V. I. Universal Size-Dependent Trend in Auger Recombination in Direct-Gap and Indirect-Gap Semiconductor Nanocrystals. *Phys. Rev. Lett.* **2009**, *102*, 177404.

(30) Vaxenburg, R.; Rodina, A.; Lifshitz, E.; Efros, A. L. Biexciton Auger Recombination in CdSe/CdS Core/Shell Semiconductor Nanocrystals. *Nano Lett.* **2016**, *16*, 2503−2511.

(31) Makarov, N. S.; Guo, S. J.; Isaienko, O.; Liu, W. Y.; Robel, I.; Klimov, V. I. Spectral and Dynamical Properties of Single Excitons, Biexcitons, and Trions in Cesium-Lead-Halide Perovskite Quantum Dots. *Nano Lett.* **2016**, *16*, 2349−2362.

(32) Eperon, G. E.; Jedlicka, E.; Ginger, D. S. Biexciton Auger Recombination Differs in Hybrid and Inorganic Halide Perovskite Quantum Dots. *J. Phys. Chem. Lett.* **2018**, *9*, 104−109.

(33) Castaneda, J. A.; Nagamine, G.; Yassitepe, E.; Bonato, L. G.; Voznyy, O.; Hoogland, S.; Nogueira, A. F.; Sargent, E. H.; Cruz, C. H. B.; Padilha, L. A. Efficient Biexciton Interaction in Perovskite Quantum Dots under Weak and Strong Confinement. *ACS Nano* **2016**, *10*, 8603−8609.

(34) Shulenberger, K. E.; Bischof, T. S.; Caram, J. R.; Utzat, H.; Coropceanu, I.; Nienhaus, L.; Bawendi, M. G. Multiexciton Lifetimes Reveal Triexciton Emission Pathway in CdSe Nanocrystals. *Nano Lett.* **2018**, *18*, 5153−5158.

(35) Bischof, T. S.; Caram, J. R.; Beyler, A. P.; Bawendi, M. G. Extracting the Average Single-Molecule Biexciton Photoluminescence Lifetime from a Solution of Chromophores. *Opt. Lett.* **2016**, *41*, 4823−4826.

(36) Amgar, D.; Yang, G.; Tenne, R.; Oron, D. Higher-Order Photon Correlation as a Tool to Study Exciton Dynamics in Quasi-2D Nanoplatelets. *Nano Lett.* **2019**, *19*, 8741−8748.

(37) Nair, G.; Zhao, J.; Bawendi, M. G. Biexciton Quantum Yield of Single Semiconductor Nanocrystals from Photon Statistics. *Nano Lett.* **2011**, *11*, 1136−1140.

(38) Ihara, T.; Kanemitsu, Y. Absorption Cross-Section Spectrum of Single CdSe/ZnS Nanocrystals Revealed through Photoluminescence Excitation Spectroscopy. *Phys. Rev. B: Condens. Matter Mater. Phys.* **2015**, *92*, 155311.

(39) Hu, F. R.; Zhang, H. C.; Sun, C.; Yin, C. Y.; Lv, B. H.; Zhang, C. F.; Yu, W. W.; Wang, X. Y.; Zhang, Y.; Xiao, M. Superior Optical Properties of Perovskite Nanocrystals as Single Photon Emitters. *ACS Nano* **2015**, *9*, 12410−12416.

(40) Hou, X. Q.; Kang, J.; Qin, H. Y.; Chen, X. W.; Ma, J. L.; Zhou, J. H.; Chen, L. P.; Wang, L. J.; Wang, L. W.; Peng, X. G. Engineering Auger Recombination in Colloidal Quantum Dots Via Dielectric Screening. *Nat. Commun.* **2019**, *10*, 1750.

(41) Yarita, N.; Tahara, H.; Ihara, T.; Kawawaki, T.; Sato, R.; Saruyama, M.; Teranishi, T.; Kanemitsu, Y. Dynamics of Charged Excitons and Biexcitons in $CsPbBr_3$ Perovskite Nanocrystals Revealed by Femtosecond Transient-Absorption and Single-Dot Luminescence Spectroscopy. *J. Phys. Chem. Lett.* **2017**, *8*, 1413−1418.

(42) Mangum, B. D.; Ghosh, Y.; Hollingsworth, J. A.; Htoon, H. Disentangling the Effects of Clustering and Multi-Exciton Emission in Second-Order Photon Correlation Experiments. *Opt. Express* **2013**, *21*, 7419−7426.

(43) Ma, X. D.; Diroll, B. T.; Cho, W. J.; Fedin, I.; Schaller, R. D.; Talapin, D. V.; Gray, S. K.; Wiederrecht, G. P.; Gosztola, D. J. Size-Dependent Biexciton Quantum Yields and Carrier Dynamics of Quasi-Two-Dimensional Core/Shell Nanoplatelets. *ACS Nano* **2017**, *11*, 9119−9127.

(44) Paulite, M.; Acharya, K. P.; Nguyen, H. M.; Hollingsworth, J. A.; Htoon, H. Inverting Asymmetric Confinement Potentials in Core/Thick-Shell Nanocrystals. *J. Phys. Chem. Lett.* **2015**, *6*, 706−711.

(45) Li, B.; Zhang, G. F.; Yang, C. G.; Li, Z. J.; Chen, R. Y.; Qin, C. B.; Gao, Y.; Huang, H.; Xiao, L. T.; Jia, S. T. Fast Recognition of Single Quantum Dots from High Multi-Exciton Emission and Clustering Effects. *Opt. Express* **2018**, *26*, 4674−4685.

(46) Park, Y. S.; Bae, W. K.; Pietryga, J. M.; Klimov, V. I. Auger Recombination of Biexcitons and Negative and Positive Trions in Individual Quantum Dots. *ACS Nano* **2014**, *8*, 7288−7296.

https://dx.doi.org/10.1021/acs.jpclett.0c02832
J. Phys. Chem. Lett. 2020, 11, 10425−10432

(47) Pietryga, J. M.; Park, Y. S.; Lim, J. H.; Fidler, A. F.; Bae, W. K.; Brovelli, S.; Klimov, V. I. Spectroscopic and Device Aspects of Nanocrystal Quantum Dots. *Chem. Rev.* **2016**, *116*, 10513−10622.

(48) Klimov, V. I. Multicarrier Interactions in Semiconductor Nanocrystals in Relation to the Phenomena of Auger Recombination and Carrier Multiplication. *Annu. Rev. Condens. Matter Phys.* **2014**, *5*, 285−316.

(49) Cordones, A. A.; Leone, S. R. Mechanisms for Charge Trapping in Single Semiconductor Nanocrystals Probed by Fluorescence Blinking. *Chem. Soc. Rev.* **2013**, *42*, 3209−21.

(50) Li, B.; Huang, H.; Zhang, G.; Yang, C.; Guo, W.; Chen, R.; Qin, C.; Gao, Y.; Biju, V. P.; Rogach, A. L.; et al. Excitons and Biexciton Dynamics in Single $CsPbBr_3$ Perovskite Quantum Dots. *J. Phys. Chem. Lett.* **2018**, *9*, 6934−6940.

(51) Wu, K. F.; Lim, J.; Klimov, V. I. Superposition Principle in Auger Recombination of Charged and Neutral Multicarrier States in Semiconductor Quantum Dots. *ACS Nano* **2017**, *11*, 8437−8447.

(52) Park, Y. S.; Guo, S. J.; Makarov, N. S.; Klimov, V. I. Room Temperature Single-Photon Emission from Individual Perovskite Quantum Dots. *ACS Nano* **2015**, *9*, 10386−10393.

(53) Hiroshige, N.; Ihara, T.; Saruyama, M.; Teranishi, T.; Kanemitsu, Y. Coulomb-Enhanced Radiative Recombination of Biexcitons in Single Giant-Shell CdSe/CdS Core/Shell Nanocrystals. *J. Phys. Chem. Lett.* **2017**, *8*, 1961−1966.

(54) Huang, X. N.; Xu, Q. F.; Zhang, C. F.; Wang, X. Y.; Xiao, M. Energy Transfer of Biexcitons in a Single Semiconductor Nanocrystal. *Nano Lett.* **2016**, *16*, 2492−2496.

https://dx.doi.org/10.1021/acs.jpclett.0c02832
J. Phys. Chem. Lett. 2020, 11, 10425−10432